
Preconditioned Score and Flow Matching

Shadab Ahamed^{*1} Eshed Gal^{*1} Simon Ghyselincks¹ Md Shahriar Rahim Siddiqui¹ Moshe Eliasof²
Eldad Haber¹

Abstract

Flow matching and score-based diffusion train vector fields under intermediate distributions p_t , whose geometry can strongly affect their optimization. We show that the covariance Σ_t of p_t governs optimization bias: when Σ_t is ill-conditioned, and gradient-based training rapidly fits high-variance directions while systematically under-optimizing low-variance modes, leading to learning that plateaus at suboptimal weights. We formalize this effect in analytically tractable settings and propose reversible, label-conditional *preconditioning* maps that reshape the geometry of p_t by improving the conditioning of Σ_t without altering the underlying generative model. Rather than accelerating early convergence, preconditioning primarily mitigates optimization stagnation by enabling continued progress along previously suppressed directions. Across MNIST latent flow matching, and additional high-resolution datasets, we empirically track conditioning diagnostics and distributional metrics and show that preconditioning consistently yields better-trained models by avoiding suboptimal plateaus.

1. Introduction

Flow matching (Lipman et al., 2023) and score-based diffusion models (Song et al., 2021; Ho et al., 2020) have become central tools for continuous-time generative modeling, achieving state-of-the-art performance across image (Cattano et al., 2025), audio (Guan et al., 2024; Xu et al., 2025a), and 3D synthesis (Wang et al., 2025; Danese et al., 2026). In both paradigms, generation is framed as the process of transporting samples from a simple reference distribution to a complex data distribution by learning a time-dependent dynamical system. Despite their empirical success, these models exhibit a persistent and increasingly well-documented

¹University of British Columbia, Vancouver, BC Canada
²University of Cambridge, Cambridge, United Kingdom. Correspondence to: Shadab Ahamed <shadab.ahamed@hotmail.com>.

Preprint. March 4, 2026.

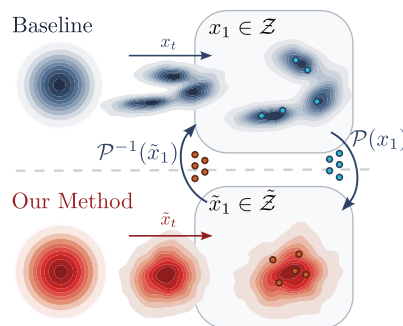


Figure 1. **(Top) Baseline:** Standard flow matching learns a transport path from a Gaussian reference to the complex data distribution $x_1 \in \mathcal{Z}$. When \mathcal{Z} exhibits strong anisotropy, the intermediate distributions $x_t \sim p_t$ inherit ill-conditioned covariances, causing gradient-based optimization to stagnate on low-variance modes. **(Bottom) Precondition-then-Match:** We introduce a reversible preconditioning operator \mathcal{P} that maps the target data to a latent representation $\tilde{\mathcal{Z}}$ that is closer to a Gaussian distribution. This transformation reshapes the geometry, ensuring that the intermediate distributions $\tilde{x}_t \sim \tilde{p}_t$ remain well-conditioned throughout the transport process, improving optimization speed. Samples are drawn by mapping back to the original data space via \mathcal{P}^{-1} , improving convergence without altering the underlying generative model capacity.

optimization phenomenon: *training loss often plateaus long before sample quality saturates* (Lin & Yang, 2025; Xu et al., 2025b).

Empirically, models that appear nearly converged under their training objective can continue to yield substantial improvements in sample fidelity for many additional epochs. This behavior suggests that slow convergence is not primarily driven by model capacity, architecture, or data availability. Instead, it points to a misalignment between the optimization objective and the aspects of the learned dynamics most relevant to generation.

Existing mitigation strategies, such as carefully tuned noise schedules (Aranguri et al., 2025), time-dependent loss reweighting (Billera et al., 2025; Diefenbacher et al., 2020), or probability flow distillation (Zhou et al., 2025), can improve sample quality in practice, but they do not directly address the underlying source of the inefficiency. These approaches often introduce additional hyperparameters or

computational overhead while leaving the core regression structure of flow and score matching unchanged. We discuss additional related work in Section A.

In this work, we show that a key contributor to slow convergence lies in the *conditioning* of the regression problems induced by flow- and score-matching objectives. At each time step, training reduces to the estimation of a vector field from samples, drawn from an intermediate distribution along the transport path. When these distributions exhibit strong anisotropy, the resulting optimization problem becomes ill-conditioned: *gradient-based methods rapidly fit high-variance directions while making only marginal progress along low-variance ones*.

To isolate and study this effect, we analyze flow matching in controlled settings where the exact transport dynamics are analytically tractable. We begin with a linear-Gaussian model problem, followed by a Gaussian-mixture extension that captures multimodality. In both cases, we show that optimization dynamics closely mirror those of gradient descent and stochastic gradient descent on ill-conditioned least-squares objectives, as commonly used in flow and score matching (Dao et al., 2023; Lipman et al., 2023; 2024). Crucially, these difficulties arise even when the model class is expressive enough to represent the exact velocity field, demonstrating that optimization, rather than approximation, is the fundamental bottleneck in convergence.

Motivated by this understanding, we discuss a novel mitigation approach that substantially improves convergence for flow matching: *preconditioning*. In its broader form, preconditioning refers to strategies that reshape the geometry of the learning problem without modifying the underlying generative process. By reducing variance imbalance across the data, preconditioning can significantly improve the convergence of the optimization algorithm, obtaining better samples with better convergence.

Contributions. Our main contributions are:

- A theoretical analysis of the optimization process in flow and score matching, revealing how data anisotropy governs the optimization speed.
- A principled preconditioning framework, inspired by numerical linear algebra, that improves convergence without changing model architecture or sampling procedures.
- We experiment with a number of datasets, from 2D points to MNIST and other image datasets, and demonstrate the novelty of our method.

2. Flow and Score Matching: Preliminaries

Continuous time generative models construct a transport from a simple reference distribution p_0 (typically Gaussian)

to a target data distribution p_1 . Rather than learning a direct map $x_0 \mapsto x_1$, these models introduce a family of intermediate distributions $\{p_t\}_{t \in [0,1]}$ obtained by the interpolation

$$x_t = s(t)x_1 + c(t)x_0, \quad (1)$$

where $s(0) = 0, s(1) = 1, c(0) = 1$ and $c(1) = 0$. The goal is to learn the dynamics governing the evolution of the probability p_t over time.

2.1. Score-based Diffusion

Score-based diffusion models (Song et al., 2021; Ho et al., 2020) define a forward noising process that gradually transforms data into noise. A parametric model $s_\theta(x, t)$ is trained to approximate the score of the intermediate distribution,

$$s_\theta(x, t) \approx \nabla_x \log p_t(x), \quad (2)$$

where p_t denotes the distribution of the noisy data at time t .

Sampling is performed by integrating the reverse-time stochastic differential equation (SDE),

$$dx_t = \left(f(x_t, t) - g(t)^2 s_\theta(x_t, t) \right) dt + g(t) dw_t, \quad (3)$$

where $g(t)$ controls the noise schedule, or equivalently, the associated probability flow ordinary differential equation (ODE),

$$\frac{dx_t}{dt} = f(x_t, t) - \frac{1}{2}g(t)^2 s_\theta(x_t, t), \quad (4)$$

which yields a deterministic transport from p_0 to p_1 .

2.2. Flow Matching

Flow matching (Lipman et al., 2023) provides an alternative formulation that avoids explicit score estimation. Instead, one directly learns the right-hand side of an ODE governing the transport between p_0 and p_1 ,

$$\frac{dx_t}{dt} = v_\theta(x_t, t), \quad x_0 \sim p_0, \quad (5)$$

Given the synthetic interpolation path between p_0 and p_1 in Equation (1), a model is trained to regress the predicted velocity $v_\theta(x_t, t)$ onto an analytically known target velocity induced by that path,

$$v^*(x_t, t) = s'(t)x_1 + c'(t)x_0.$$

In the standard conditional flow matching setting, training minimizes,

$$\mathcal{L}_{\text{CFM}}(\theta) = \mathbb{E}_{x_0, x_1} \int_0^1 \|v_\theta(x_t, t) - v_t^*(x_t, t)\|^2 dt. \quad (6)$$

This optimization problem can be thought of as a generic regression that aims to approximate $v_t^*(x_t, t)$ by the learned vector field $v_\theta(x_t, t)$.

2.3. A Unified Optimization Perspective

Despite differences in parameterization, both score and flow matching reduce to time-indexed least-squares regression under intermediate distributions p_t . At each time t , training approximates a target vector field using samples from p_t , with optimization performed via stochastic gradient descent.

From this perspective, optimization behavior is governed not only by model expressiveness, but also by the geometric properties of p_t that enter the regression objective. Crucially, the geometry of p_t , especially its covariance Σ_t , affects convergence. When Σ_t is ill-conditioned, the regression becomes poorly conditioned, leading to rapid convergence in some directions and slow or stalled progress in others (Boyd & Vandenberghe, 2004). In stochastic settings, this effect is further exacerbated by gradient noise, leading to premature plateaus despite nonzero optimal error (Bottou et al., 2016).

In Section 3, we analyze Gaussian and Gaussian mixture models for which the exact score or flow is analytically known, revealing that anisotropic covariances directly impair optimization, independent of model capacity.

3. Gaussian Transport Model: A Solvable Case of Optimization Difficulty

We study a simplified setting where both the base and target distributions are Gaussian, and the ground truth transport is linear. This fully solvable model reveals that optimization difficulties in flow and score matching stem from conditioning on intermediate distributions, mirroring gradient descent on ill-conditioned quadratics (Shapiro et al., 2009). We highlight these phenomena in more detail in Section B and in Figure 6 we visualize the evolution of covariance structure, condition numbers, and the resulting impact on gradient descent dynamics and learned score and vector fields.

3.1. Setup: Ill-conditioned Target Covariance

Let the base distribution be $x_0 \sim \mathcal{N}(0, I)$, and the target distribution be $x_1 \sim \mathcal{N}(0, H)$, where $H \in \mathbb{R}^{d \times d}$ is symmetric and positive definite. We write the eigen-decomposition, $H = U\Lambda U^\top$, with orthogonal U and $\Lambda = \text{diag}(\lambda_1, \dots, \lambda_d)$, $\lambda_i > 0$. We say that H is *ill-conditioned* if its condition number,

$$\kappa(H) = \frac{\lambda_{\max}(H)}{\lambda_{\min}(H)} = \frac{\max_i \lambda_i}{\min_i \lambda_i} \quad (7)$$

is large. Geometrically, this means that samples from x_1 exhibit highly anisotropic variability: along eigendirections corresponding to larger λ_i , the distribution has larger variance, while directions associated with smaller λ_i are tightly concentrated. Such anisotropy leads to strong disparities in curvature across directions. This disparity directly impacts

optimization, as gradient-based learning tends to progress more rapidly along well-conditioned directions, while converging slowly along directions associated with small variance (Nocedal & Wright, 1999).

Using a simple path between x_0 and x_1 ,

$$x_t = (1 - t)x_0 + tx_1, \quad t \in [0, 1]. \quad (8)$$

For each fixed t , x_t is a Gaussian random variable with mean zero and covariance that we will compute explicitly below.

3.2. Analytic Score and Velocity in the Gaussian Case

Before formulating the learning problem, we first compute the exact score and velocity fields induced by the interpolation, $x_t = (1 - t)x_0 + tx_1$, $x_0 \sim \mathcal{N}(0, I)$, $x_1 \sim \mathcal{N}(0, H)$. Because x_0 and x_1 are jointly Gaussian and x_t is their affine combination, the conditional distribution of $(x_1 - x_0)$ given x_t is Gaussian and linear in x_t . In particular, both the score and the flow velocity at time t are linear functions of x_t .

Score. The marginal distribution of x_t is Gaussian with covariance,

$$\Sigma_t := \mathbb{E}[x_t x_t^\top] = (1 - t)^2 I + t^2 H. \quad (9)$$

Using the identity for the gradient of the log of a normal distribution, we have,

$$\nabla_x \log p_t(x_t) = -\Sigma_t^{-1} x_t. \quad (10)$$

Velocity. The probability–flow ODE associated with the linear interpolation satisfies, $dx_t/dt = x_1 - x_0$. Taking conditional expectation with respect to x_t gives the exact velocity field, $v_t^*(x_t) = \mathbb{E}[x_1 - x_0 | x_t] = A^*(t) x_t$, for some matrix $A^*(t) \in \mathbb{R}^{d \times d}$ depending only on t and H . Using standard Gaussian conditioning,

$$\begin{aligned} A^*(t) &= \text{Cov}(x_1 - x_0, x_t) \Sigma_t^{-1} \\ &= (tH - (1 - t)I) ((1 - t)^2 I + t^2 H)^{-1}. \end{aligned} \quad (11)$$

We note that both the score and the velocity are *exactly linear* in x_t . Therefore, the model class $v_\theta(x_t, t) = A(t) x_t$, is expressive enough to represent the true flow *without approximation error*. Any optimization difficulty observed in this section cannot be attributed to model misspecification, non-linear effects, or limited parameterization – *it arises solely from the statistics of the regression problem at time t* .

Key observation. Even when the true flow is exactly representable, optimization can be arbitrarily slow due solely to the ill-conditioning of the intermediate covariance Σ_t , as we quantify below, which suppresses learning along low-variance directions.

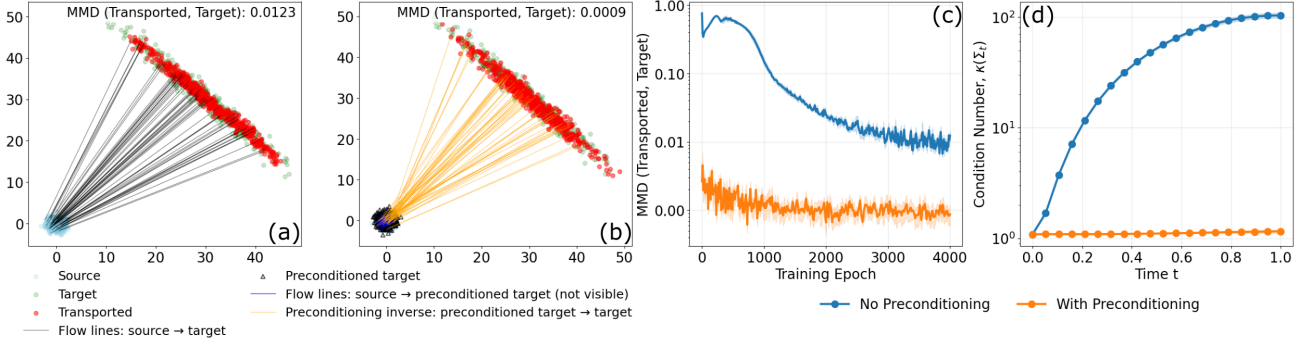


Figure 2. Comparison of flow matching without and with preconditioning on a 2D Gaussian transport task. (a) Standard flow matching transports samples from the source Gaussian (blue) to the elongated target Gaussian (green). (b) Preconditioned flow matching transports samples to a whitened target (black triangles) (flow lines not visible), then inverts the preconditioning to obtain the transported samples. (c) Preconditioning avoids early optimization stagnation and achieves a lower Maximum Mean Discrepancy (MMD) between the target and the transported distribution. (d) Condition number of the learned transport map over time for both methods. The preconditioned approach achieves lower condition numbers, improving sample alignment and optimization stability.

This observation motivates the learning problem studied in Section 3.3: the goal is to recover the exact matrix $A^*(t)$ from data by minimizing mean squared error. As we will show, even in this analytically solvable Gaussian setting, where the target flow is completely linear, gradient-based optimization can be unexpectedly slow depending on the structure of H .

3.3. Linear Regression Objective and Exact Minimizer

At a fixed time t , we consider a linear predictor for the velocity field, $v_\theta(x_t, t) = A(t)x_t$, where $A(t) \in \mathbb{R}^{d \times d}$ is a parameter matrix. As a simple and analytically tractable proxy for flow matching, we take the target velocity to be $v_t^* = x_1 - x_0$, and define the mean-squared error objective,

$$\mathcal{L}(A(t)) = \mathbb{E}[\|A(t)x_t - (x_1 - x_0)\|^2]. \quad (12)$$

This objective is quadratic and therefore the optimal solution, $A^*(t)$, can be obtained by solving the linear system,

$$A^*(t)\Sigma_t = tH - (1-t)I, \quad (13)$$

where Σ_t is defined in Equation (9). The full derivation for Σ_t , the cross-covariance, and the normal equations is provided in Section B.1.

3.4. Condition Number and Convergence

The regression problem in Equation (12) is governed by the covariance matrix Σ_t , which appears both in the normal equations and in the gradient dynamics. We characterize its spectrum and conditioning in terms of t and the eigenvalues of H . Since Σ_t and H share the same eigenvectors, the eigenvalues of Σ_t are,

$$\sigma_i(t) = (1-t)^2 + t^2\lambda_i, \quad i = 1, \dots, d, \quad (14)$$

where $\{\lambda_i\}_{i=1}^d$ are the eigenvalues of H . A derivation for this spectral form is provided in Section B.2. The condition number of Σ_t is therefore,

$$\kappa(\Sigma_t) = \frac{\max_i \sigma_i(t)}{\min_i \sigma_i(t)} = \frac{(1-t)^2 + t^2\lambda_{\max}}{(1-t)^2 + t^2\lambda_{\min}}. \quad (15)$$

Several regimes are informative. For $t = 0$, we have $\Sigma_0 = I$ and $\kappa(\Sigma_0) = 1$, corresponding to perfect conditioning. For $t = 1$, $\Sigma_1 = H$ and $\kappa(\Sigma_1) = \kappa(H)$. For intermediate $t \in (0, 1)$, the condition number interpolates smoothly between these two extremes and converges to $\kappa(H)$ as $t \rightarrow 1$.

When H is ill-conditioned, and t is not too close to zero, Σ_t exhibits a large condition number. As we show next, this directly leads to the slow convergence of gradient-based optimization, even though the model, i.e., the neural network, can represent the exact solution.

In the context of Gradient Descent, the effect of the condition number on the convergence behavior for gradient-based methods is well-studied in the literature (Nocedal & Wright, 1999; Boyd & Vandenberghe, 2004). In particular, we have that the number of iterations k for the solution of the problem scales as,

$$k \approx \frac{\log(1/\varepsilon)}{-\log \rho} \approx \frac{1}{2\eta\sigma_{\min}(t)} \log \frac{1}{\varepsilon}. \quad (16)$$

When Σ_t is ill-conditioned, $\sigma_{\min}(t)$ is small and $\sigma_{\max}(t)$ is large. The learning rate must satisfy $\eta < 1/\sigma_{\max}(t)$, which forces ρ close to 1 and results in extremely slow convergence along low variance directions. This behavior mirrors the classical convergence theory of gradient descent on ill-conditioned quadratic objectives (Boyd & Vandenberghe, 2004).

In the context of Stochastic Gradient Descent (SGD), the problem of ill-conditioning becomes even more acute

(Shapiro et al., 2009). We briefly summarize how stochasticity affects the error dynamics, deferring derivations to Section B.4.

At a fixed time t , the SGD error admits a decomposition into independent modes aligned with the eigenvectors of Σ_t . In each eigendirection i , the scalar error component $e_{i,m}$ follows a linear stochastic recursion of the form,

$$e_{i,m+1} = (1 - 2\eta\sigma_i(t))e_{i,m} + \zeta_{i,m}, \quad (17)$$

where $\zeta_{i,m}$ is a zero-mean noise term whose variance depends on the gradient variability in direction i .

In steady state, the variance of $e_{i,m}$ satisfies,

$$\text{Var}(e_{i,\infty}) \propto \frac{\eta}{\sigma_i(t)}. \quad (18)$$

Thus, directions associated with small eigenvalues $\sigma_i(t)$ suffer a two-fold disadvantage: (i) they contract very slowly due to the small deterministic factor $2\eta\sigma_i(t)$; and (ii) they accumulate larger stochastic fluctuations due to the inverse dependence of the steady state variance on $\sigma_i(t)$. As a result, low variance directions dominate both convergence speed and final accuracy under SGD.

Alternative Optimization Techniques. Ill-conditioning has similar effects virtually on any first order method (methods such as Adam (Kingma & Ba, 2014)), that do not approximately invert the Hessian (Nocedal & Wright, 1999; Bottou et al., 2016), and therefore the effects discussed above are to be observed on virtually all common techniques that are used for the solution of the regression problem in Equation (12).

3.5. Extension to Gaussian Mixture Model

While the Gaussian case analysis in Sections 3.1 to 3.4 is simple, it also extends to the more complex setting of a Gaussian mixture. Detailed derivations for this subsection are provided in Section C.

Let the target distribution be a mixture of K Gaussians with zero mean,

$$x_1 \sim \sum_{k=1}^K \pi_k \mathcal{N}(0, H_k), \quad \pi_k > 0, \quad \sum_{k=1}^K \pi_k = 1, \quad (19)$$

with base distribution $x_0 \sim \mathcal{N}(0, I)$ and interpolation $x_t = (1-t)x_0 + tx_1$. As in Section 3.2, the score and probability flow velocity remain analytic, but now take the form of mixtures of linear maps weighted by posterior components.

Assuming perfect component assignment, optimization decomposes into K regression subproblems, each governed by the component-specific covariance,

$$\Sigma_{t,k} = (1-t)^2 I + t^2 H_k, \quad (20)$$

with the eigenvalues of $\Sigma_{t,k}$ given by $\sigma_{k,i}(t) = (1-t)^2 + t^2 \lambda_{k,i}$, where $\{\lambda_{k,i}\}_{i=1}^d$ are the eigenvalues of H_k . Consequently, both gradient descent and stochastic gradient descent converge at rates controlled by the optimization problem,

$$\min_{k,i} \sigma_{k,i}(t), \quad (21)$$

i.e., by the smallest eigenvalue across all mixture components. Even if most components are well-conditioned, a single poorly conditioned component dominates the global convergence rate and steady state error. Thus, multimodality exacerbates the optimization bottleneck identified in Section 3: *training speed and final accuracy are governed by the hardest component rather than by average data geometry.*

Key observation. In Gaussian mixtures, optimization is controlled by the *worst-conditioned component*. Even if most components are well-behaved and the model is expressive, a single anisotropic component can dominate convergence speed and final error, causing training to plateau. Multimodality, therefore, amplifies conditioning effects rather than averaging them out.

4. Preconditioning: A General Solution to Optimization Bottlenecks

The analyses in Sections 3 and 3.5 show that the convergence rate of gradient-based training is governed by the smallest eigenvalue of the covariance matrices Σ_t (Gaussian case) or $\Sigma_{t,k}$ (GMM case). When these matrices are ill-conditioned, the optimization becomes slow, even though the model class is expressive enough to represent the exact flow. This phenomenon mirrors classical optimization in linear algebra, where gradient descent struggles on poorly conditioned systems. In this section, we introduce a general preconditioning framework that improves convergence by transforming the data distribution before applying flow matching.

In linear algebra, solving a linear system $Mx = b$, with gradient descent, is practical only when M is well-conditioned. When the linear system is ill-conditioned, it is common to *precondition* the problem, that is, transforming it to a form,

$$(\widehat{M}^{-1}M)x = \widehat{M}^{-1}b, \quad (22)$$

where \widehat{M} is a preconditioner. Optimally, $\widehat{M} = M$; however, this is impractical. In practice, \widehat{M} approximates M in some sense and is much easier to invert. The point is that the new problem with the linear system $\widehat{M}^{-1}M$ as a system matrix, has a much better condition number and therefore is much more amenable to the convergence of iterative methods and in particular to gradient-based methods.

Preconditioning is a well-studied field (see Benzi (2002); Saad (1992); Golub & Ye (2000)) with a wide variety of methods that are problem-dependent. Our goal here is to construct an analogous preconditioning transformation for flow and score matching: instead of predicting the flow for the original target distribution x_1 directly, we use an invertible preconditioner operator \mathcal{P} and define a new distribution $\tilde{x}_1 = \mathcal{P}x_1$ that is closer to Gaussian. The regression problem associated with \tilde{x}_1 is then much better conditioned, preventing early optimization stagnation and leading to sub-optimal solutions. As a result, our flow matching training problem can be divided into the following two steps,

Precondition-then-Match Framework:

1. Apply a learned preconditioner \mathcal{P} to map $x_1 \mapsto \tilde{x}_1$ with more isotropic structure.
2. Use standard flow matching to model the flow $\mathcal{N}(0, I) \rightarrow \tilde{x}_1$.

See Figure 2 for an illustration of how preconditioning improves sample alignment and conditioning in a simple 2D transport task from a standard Gaussian to an elongated Gaussian, and also mitigates optimization stagnation to sub-optimal solutions.

We now provide theoretical justification for the benefits of preconditioning in a simplified setting. The following result shows how preconditioning can dramatically accelerate convergence in a basic least squares problem, illustrating the same principles at play in flow matching.

Theorem 4.1 (Preconditioning Improves Convergence). *Consider the linear least squares objective*

$$\mathcal{L}(A) = \mathbb{E}[\|Ax - y\|^2],$$

where $x \in \mathbb{R}^d$, $y \in \mathbb{R}^d$, and $\Sigma = \mathbb{E}[xx^\top]$ is positive definite with condition number $\kappa(\Sigma) = \lambda_{\max}(\Sigma)/\lambda_{\min}(\Sigma)$. Let A^* denote the optimal solution and let gradient descent be used to minimize $\mathcal{L}(A)$. Then,

- **Without preconditioning:** gradient descent converges linearly at rate,

$$\|A_k - A^*\|_F \leq (1 - 2\eta\lambda_{\min}(\Sigma))^k \|A_0 - A^*\|_F,$$

where $\eta < 1/\lambda_{\max}(\Sigma)$, requiring $\mathcal{O}(\kappa \log(1/\varepsilon))$ steps to reach error ε (here, $\|\cdot\|_F$ denotes the Frobenius norm).

- **With preconditioning:** let $\mathcal{P} = \Sigma^{-1/2}$ and define $\tilde{x} = \mathcal{P}x$. Then gradient descent on the transformed problem, $\tilde{\mathcal{L}}(A) = \mathbb{E}[\|A\tilde{x} - y\|^2]$ converges at a rate,

$$\|A_k - A^*\|_F \leq (1 - 2\eta)^k \|A_0 - A^*\|_F,$$

with no dependence on κ , and requires only $\mathcal{O}(\log(1/\varepsilon))$ steps.

This result formally explains why preconditioning alleviates optimization bottlenecks arising from ill-conditioned input geometry. A full proof is provided in Section D.1.

Importantly, our proposed approach does not represent a single algorithm but rather many possible algorithms. Similarly to preconditioners for linear systems (Benzi et al., 2005), a preconditioner in our work can be a solver that is used to transform the data from its original form to more Gaussian-like. Preconditioning can be achieved in many different ways, and while we propose two methods below, we foresee other methods that can be tailored to specific datasets. We provide an expanded discussion in Section 6.

4.1. Normalizing Flow Preconditioner

One common technique for transforming data sampled from a target distribution into a Gaussian is Normalizing Flows (Rothotto & Haber, 2021; Kobyzev et al., 2020; Papamakarios et al., 2019). The main idea is to use a reversible transformation \mathcal{P}_θ to transform the data, $\tilde{x}_1 = \mathcal{P}_\theta(x)$. If $\tilde{x}_1 \sim \mathcal{N}(0, I)$, then the distribution of x_1 can be computed by the change-of-variables formula,

$$p(x_1) = \mathcal{N}(\mathcal{P}_\theta(x_1); 0, I) \cdot |\det D\mathcal{P}_\theta(x_1)|, \quad (23)$$

where $D\mathcal{P}_\theta$ denotes the Jacobian. Maximum-likelihood training aims to maximize $p(x_1)$ or minimize its negative log over the observed data, which leads to the following optimization problem,

$$\min_{\theta} \mathbb{E}_{x_1 \sim p_1} \left[\frac{1}{2} \|\mathcal{P}_\theta(x_1)\|^2 - \log |\det D\mathcal{P}_\theta(x_1)| \right]. \quad (24)$$

While normalizing flows offer a compelling generative modeling approach, they require invertible transformations with tractable log-Jacobian determinants. This restricts them to a less expressive family compared to models like UNet (Ronneberger et al., 2015) or DiT (Croitoru et al., 2023), making them less popular than flow matching or diffusion methods. Nonetheless, such flows can be used as excellent preconditioners to flow matching, transforming the data from its original form to a more Gaussian representation, that makes flow matching much more effective.

4.2. Flow Matching Preconditioner

A second approach to designing a preconditioner is to learn a low-capacity flow that uses a small, relatively inexpensive network to transform the data. In this case, we first solve the optimization problem in Equation (6), and train a low-capacity network for a velocity field $v_\eta(x_t, t)$. We then

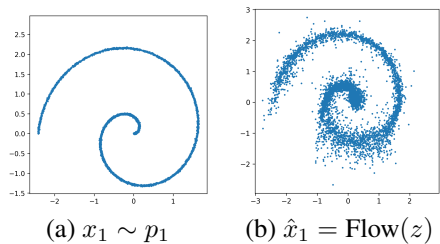


Figure 3. **Flow matching without preconditioning.** (a) Ground-truth Swiss roll samples $x_1 \sim p_1$. (b) Generated samples \hat{x}_1 obtained by transporting Gaussian source z through a learned flow. The structural mismatch highlights the challenge of learning complex transport maps without preconditioning.

integrate the data,

$$\frac{dx}{dt} = -v_\eta(x, t) \quad x(t=0) \sim p_1(x), \quad t \in [0, 1]. \quad (25)$$

Let \mathcal{P}_η be the pushforward operator from x_1 to the final state \tilde{x}_1 . The new data, $\tilde{x}_1 = \mathcal{P}_\eta(x_1)$ at $t = 1$ is much more Gaussian-like than the original data x_1 . We then use a standard flow matching to compute a velocity model from \tilde{x}_1 to a Gaussian.

Particular choices of low-capacity networks that can be used as preconditioners are presented in our numerical experiments 5. Such networks are typically problem-dependent.

5. Experiments

Preconditioning is a new concept in the context of flow matching. Our goal here is to illustrate its effectiveness on problems where its effect can be tested. We emphasize that large, diverse datasets (such as ImageNet) require special attention and preconditioners. Designing an optimal preconditioner for such datasets is beyond the scope of this paper. Nonetheless, we show the effectiveness of our approach for a number of commonly used image datasets, such as MNIST, LSUN Churches (Yu et al., 2015), Oxford Flowers-102 (Nilsback & Zisserman, 2008), and AFHQ Cats (Choi et al., 2020). We first present our experiments with 2D flows, where the effect of each preconditioner can be easily observed, and then also show results on image datasets.

5.1. 2D Point Clouds

To build intuition and isolate algorithmic behavior of the proposed preconditioning strategy, we begin with 2D experiments since low-dimensional settings allow for direct visualization of densities, transport maps, and trajectories.

We study the Swiss roll, a curved, anisotropic, non-Gaussian manifold with severe scale separation, as a testbed for evaluating preconditioning methods. Even with small isotropic noise, its geometry is challenging: elongated along the manifold and tightly concentrated transversely. Preconditioning

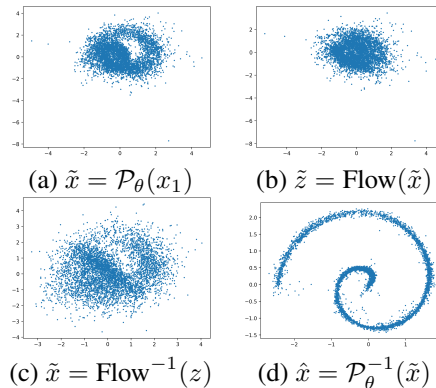


Figure 4. **Flow matching preconditioned by a normalizing flow.** (a) The data x_1 (Swiss Roll) is pushed forward by normalizing flow to \tilde{x}_1 . (b) The points \tilde{x}_1 computed in (a) are integrated with a learned velocity field to Gaussian points \tilde{z} . (c) Random Gaussian points z are pushed backwards using the flow to obtain \tilde{x}_1 . (d) The points \tilde{x}_1 in (c) are pushed backwards using the normalizing flow.

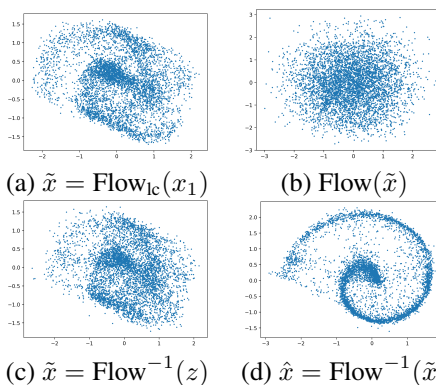


Figure 5. **Flow matching preconditioned by a low accuracy flow.** (a) The data (Swiss roll) is pushed forward by a preconditioner, low-accuracy flow. (b) The points computed in (a) are integrated with a learned velocity field to a Gaussian. (c) Random Gaussian points are pushed backwards using the high-capacity flow. (d) The points in (c) are pushed backwards using the low-capacity flow.

here serves as geometric isotropization, aiming to reduce anisotropy and simplify the structure to facilitate easier transport toward a Gaussian. As a baseline, we use standard flow matching to map a Gaussian to the Swiss roll, the results for which are presented in Figure 3. We then use both a normalizing flow and a flow-matching-based model to precondition the problem.

Normalizing Flow Preconditioner. Figure 4 shows that normalizing flow (NF) significantly improves generation quality over the standard non-preconditioned flow matching (Figure 3). While the pushforward $\tilde{x} = \mathcal{P}_\theta(x_1)$ in Figure 4 (a) isn't perfectly Gaussian either, it is far more isotropic (and closer to Gaussian), allowing the second-stage flow (b) to operate on a simpler geometry. In inference, Gaussian samples are pulled back via the learned flow (c) and the inverse NF (d), recovering the original distribution more

Table 1. Sliced-Schaefer distances for the Swiss roll dataset. The top row compares generated samples with ground truth; the bottom row measures how Gaussian the pushed data is. Lower is better.

Direction	No preconditioner	NF preconditioner	Flow preconditioner
$z \rightarrow x_1$	1.11×10^{-1}	5.8×10^{-2}	7.2×10^{-2}
$x_1 \rightarrow z$	8.1×10^{-1}	3.1×10^{-1}	3.4×10^{-1}

faithfully, as compared to Figure 3 (b).

Flow Matching Preconditioner. In our second experiment, we use a low-capacity flow Flow_{1c} with just 168 parameters as a preconditioner. As shown in Figure 5, even such a lightweight model improves the performance of a downstream high-capacity flow, similar to the normalizing flow case in Figure 4.

To evaluate the effect of preconditioning quantitatively, we compute the Sliced-Schaefer distance between point clouds in both directions: $x_1 \rightarrow z$ (data to Gaussian) and $z \rightarrow x_1$ (Gaussian to data). Results in Table 1 show that both preconditioners improve upon the baseline, with normalizing flow performing the best. Its distinct transformation is likely to complement flow matching by reducing the effective null space of the standard flow. We provide additional experiments in 2D for the Checkerboard to Swiss roll transport problem in Section G.1 and Figure 11.

5.2. MNIST

We evaluate our method on MNIST using a two-stage approach in the latent space of a VAE (trained from scratch with 64 latent dimensions). The main flow model is a conditional MLP-based vector field trained with flow matching using sine-cosine interpolation. We compare two preconditioners: a normalizing flow trained via maximum-likelihood, and a low-capacity flow trained with flow matching. FID scores between decoded samples and real images are used for evaluation. Full architectural and training details are provided in the Section F.1. Quantitative results are provided in Table 2, which shows that preconditioning significantly improves the perceptual quality of the generated images for the MNIST data. Some qualitative visualizations are presented in Figure 7. Also, see Figure 12 for a comparison of condition numbers $\kappa(\Sigma_t)$ across time t , showing that both preconditioning methods significantly reduce ill-conditioning throughout the transport.

5.3. High-Resolution Image Synthesis

We evaluate flow-based preconditioning using a UNet backbone across varying resolutions. Experiments are conducted on Oxford Flowers-102 (Nilsback & Zisserman, 2008) and LSUN Churches (Yu et al., 2015) at 256×256 resolution, and extended to the AFHQ Cats dataset (Choi et al., 2020)

Table 2. FID scores for the MNIST dataset comparing the flow matching performance in the latent space of VAE, without preconditioning, with a normalizing flow (NF) preconditioner, and with a flow matching preconditioner. Lower FID indicates better performance.

Dataset	No preconditioner	NF preconditioner	Flow preconditioner
MNIST	13.83	2.62	6.95

Table 3. FID scores for the datasets, LSUN Churches, Oxford Flowers-102, and AFHQ Cats, comparing the flow matching in the latent space of VAE, without and with a flow matching preconditioning. Lower FID indicates better performance.

Dataset	No preconditioner	Flow preconditioner
LSUN Churches	19.53	14.47
Oxford Flowers-102	23.82	22.64
AFHQ Cats	8.41	7.75

at 512×512 resolution to assess scalability. As shown in Table 3, preconditioning yields consistent FID improvements over standard flow matching. The baseline is trained until convergence, ensuring that these gains reflect improved optimization rather than undertraining. Additional implementation details are provided in Section F.

Preconditioning is implemented using an additional flow model. We do not use normalizing flows as preconditioners for those datasets, since their invertibility constraints and architectural restrictions make them less compatible with real-world complex data (Papamakarios et al., 2019). In contrast, flow-based preconditioning provides a flexible, architecture-aligned mechanism for improving conditioning without modifying the core generative model. Qualitative results in Section E further show that the additional flow corrects residual artifacts and visually improves samples that standard flow matching fails to refine.

6. Discussion and Conclusion

In practice, flow and score networks are nonlinear and high-dimensional, making direct spectral analysis infeasible. Still, our linear toy model highlights core optimization barriers induced by data covariance. It reveals how poor conditioning can significantly hinder convergence in both gradient descent and SGD, even when the model is expressive enough to learn the target. These insights are supported by experiments showing that preconditioning improves both optimization behavior and sample quality. Future directions include learning time-dependent preconditioners $A(t)$, empirically verifying how t -weighted sampling and per- t learning rates affect convergence and sample quality, extending the analysis to latent-variable models, and studying SGD dynamics in nonlinear networks via local linearization.

Impact Statement. This work is methodological in nature and focuses on improving the optimization behavior of score-based diffusion and flow matching models through principled preconditioning. By clarifying the roles of data geometry and conditioning in these generative frameworks, the proposed analysis and methods aim to make training more stable and efficient without introducing new modeling assumptions or expanding into new application domains. The techniques studied here do not inherently introduce new societal risks beyond those already associated with existing generative image models. We expect this work to primarily benefit researchers and practitioners by providing clearer diagnostics and design principles for training continuous-time generative models more reliably.

References

- Aranguri, S., Biroli, G., Mezard, M., and Vanden-Eijnden, E. Optimizing noise schedules of generative models in high dimensions. *arXiv preprint arXiv:2501.00988*, 2025.
- Benzi, M. Preconditioning techniques for large linear systems: A survey. *Journal of Computational Physics*, 182(2):418–477, 2002. ISSN 0021-9991. doi: <https://doi.org/10.1006/jcph.2002.7176>.
- Benzi, M., Golub, G. H., and Liesen, J. Numerical solution of saddle point problems. *Acta numerica*, 14:1–137, 2005.
- Billera, L., Nordlinder, H. N., and Murrell, B. Time dependent loss reweighting for flow matching and diffusion models is theoretically justified. *arXiv preprint arXiv:2511.16599*, 2025.
- Bottou, L., Curtis, F. E., and Nocedal, J. Optimization methods for large-scale machine learning. *arXiv preprint arXiv:1606.04838*, 2016.
- Boyd, S. and Vandenberghe, L. *Convex optimization*. Cambridge University press, 2004.
- Caetano, F., Viviers, C., With, P. H. N. D., and van der Sommen, F. Symmetrical flow matching: Unified image generation, segmentation, and classification with score-based generative models. *arXiv preprint arXiv:2506.10634*, 2025.
- Cao, W. and Zhang, W. An analysis and solution of ill-conditioning in physics-informed neural networks. *Journal of Computational Physics*, 520:113494, 2025. ISSN 0021-9991.
- Choi, Y., Uh, Y., Yoo, J., and Ha, J.-W. Stargan v2: Diverse image synthesis for multiple domains. In *Proceedings of the IEEE Conference on Computer Vision and Pattern Recognition*, 2020.
- Croitoru, F.-A., Hondru, V., Ionescu, R. T., and Shah, M. Diffusion models in vision: A survey. *IEEE Transactions on Pattern Analysis and Machine Intelligence*, 2023.
- Danese, D., Lombardi, A., Attimonelli, M., Fasano, G., and Noia, T. D. Flowlet: Conditional 3d brain mri synthesis using wavelet flow matching. *arXiv preprint arXiv:2601.05212*, 2026.
- Dao, Q., Phung, H., Nguyen, B., and Tran, A. Flow matching in latent space. *arXiv preprint arXiv:2307.08698*, 2023.
- Dauphin, Y. N., Pascanu, R., Gulcehre, C., Cho, K., Ganguli, S., and Bengio, Y. Identifying and attacking the saddle point problem in high-dimensional non-convex optimization. In *Advances in Neural Information Processing Systems*, 2014.
- Diefenbacher, S., Eren, E., Kasiyczka, G., Korol, A., Nachman, B., and Shih, D. DctrGAN: Improving the precision of generative models with reweighting. *Journal of Instrumentation*, 2020.
- Dinh, L., Sohl-Dickstein, J., and Bengio, S. Density estimation using real nvp. In *ICLR*, 2017.
- Golub, G. and Ye, Q. Inexact preconditioned conjugate gradient method with inner-outer iteration. *SIAM J. Scient. Comp.*, 21:1305–1320, 2000.
- Guan, W., Wang, K., Zhou, W., Wang, Y., Deng, F., Wang, H., Li, L., Hong, Q., and Qin, Y. Lafma: A latent flow matching model for text-to-audio generation. *Interspeech*, 2024.
- Ho, J., Jain, A., and Abbeel, P. Denoising diffusion probabilistic models. In *Advances in Neural Information Processing Systems (NeurIPS)*, 2020.
- Karras, T., Aittala, M., Aila, T., and Laine, S. Elucidating the design space of diffusion-based generative models. *Neural Information Processing Systems*, 2022.
- Kingma, D. P. and Ba, J. Adam: A method for stochastic optimization. *International Conference on Learning Representations*, 2014.
- Kingma, D. P. and Welling, M. Auto-encoding variational bayes. *International Conference on Learning Representations*, 2013.
- Kobyzev, I., Prince, S. J., and Brubaker, M. A. Normalizing flows: An introduction and review of current methods. *IEEE transactions on pattern analysis and machine intelligence*, 43(11):3964–3979, 2020.

- Lazzarino, L., Nakatsukasa, Y., and Zerbinati, U. Preconditioned normal equations for solving discretised partial differential equations. *arXiv preprint arXiv:2502.17626*, 2025.
- Lin, S. and Yang, X. Diffusion model with perceptual loss. *arXiv preprint arXiv:2401.00110v7*, 2025.
- Lipman, Y., Chen, R. T. Q., Ben-Hamu, H., Nickel, M., and Le, M. L. Flow matching for generative modeling. In *International Conference on Learning Representations (ICLR)*, 2023.
- Lipman, Y., Havasi, M., Holderrieth, P., Shaul, N., Le, M., Karrer, B., Chen, R. T., Lopez-Paz, D., Ben-Hamu, H., and Gat, I. Flow matching guide and code. *arXiv preprint arXiv:2412.06264*, 2024.
- Nilsback, M.-E. and Zisserman, A. Automated flower classification over a large number of classes. In *Proceedings of the Indian Conference on Computer Vision, Graphics and Image Processing (ICVGIP)*, 2008.
- Nocedal, J. and Wright, S. *Numerical Optimization*. Springer, 1999.
- Papamakarios, G., Nalisnick, E., Rezende, D. J., Mohamed, S., and Lakshminarayanan, B. Normalizing flows for probabilistic modeling and inference. *Journal of Machine Learning Research*, 2019.
- Quiryne, R. and Di Cairano, S. Presas: Block-structured preconditioning of iterative solvers within a primal active-set method for fast mpc. *arXiv preprint arXiv:1912.02122v2*, 2020.
- Rombach, R., Blattmann, A., Lorenz, D., Esser, P., and Ommer, B. High-resolution image synthesis with latent diffusion models. In *Proceedings of the IEEE/CVF conference on computer vision and pattern recognition*, pp. 10684–10695, 2022.
- Ronneberger, O., Fischer, P., and Brox, T. U-net: Convolutional networks for biomedical image segmentation. In *International Conference on Medical image computing and computer-assisted intervention*, pp. 234–241. Springer, 2015.
- Ruthotto, L. and Haber, E. An introduction to deep generative modeling. *GAMM-Mitteilungen*, 44(2):e202100008, 2021.
- Saad, Y. Analysis of some krylov subspace approximations to the matrix exponent operator. *SIAM J. Numer Anal*, 29, 1992.
- Saad, Y. *Iterative Methods for Sparse Linear Systems*. SIAM, 2003.
- Shapiro, A., Dentcheva, D., and Ruszczyński, D. *Lectures on Stochastic Programming: Modeling and Theory*. SIAM, Philadelphia, 2009.
- Song, Y., Sohl-Dickstein, J., Kingma, D. P., Kumar, A., Ermon, S., and Poole, B. Score-based generative modeling through stochastic differential equations. In *International Conference on Learning Representations (ICLR)*, 2021.
- Trefethen, L. N. and Bau, D. *Numerical Linear Algebra*. SIAM, 1997.
- Wang, J., Reynaud, H., Erick, F. X., and Kainz, B. Ctflo: Video-inspired latent flow matching for 3d ct synthesis. *arXiv preprint arXiv:2508.12900*, 2025.
- Xu, X., Mei, J., Zheng, Z., Tao, Y., Xie, Z., Zhang, Y., Liu, H., Wu, Y., Yan, M., Wu, W., Zhang, C., and Wu, M. Uniflow-audio: Unified flow matching for audio generation from omni-modalities. *arXiv preprint arXiv:2509.24391*, 2025a.
- Xu, Y., Luo, S., Wang, L., He, D., and Liu, C. Diagnosing and improving diffusion models by estimating the optimal loss value. *arXiv preprint arXiv:2506.13763*, 2025b.
- Ye, Q. Preconditioning for accelerated gradient descent optimization and regularization. *arXiv preprint arXiv:2410.00232v2*, 2024.
- Yu, F., Seff, A., Zhang, Y., Song, S., Funkhouser, T., and Xiao, J. Lsun: Construction of a large-scale image dataset using deep learning with humans in the loop. In *Proceedings of the IEEE Conference on Computer Vision and Pattern Recognition (CVPR)*, 2015.
- Zhai, S., Zhang, R., Nakkiran, P., Berthelot, D., Gu, J., Zheng, H., Chen, T., Bautista, M. A., Jaitly, N., and Susskind, J. Normalizing flows are capable generative models. *arXiv preprint arXiv:2412.06329v3*, 2025.
- Zhou, M., Gu, Y., Zheng, H., Song, L., He, G., Zhang, Y., Hu, W., and Yang, Y. Score distillation of flow matching models. *arXiv preprint arXiv:2509.25127*, 2025.

A. Additional Related Work

Generative Models. Generative models aim to learn complex data distributions in order to synthesize realistic samples. Early approaches include explicit density models such as variational autoencoders and autoregressive models, which provide principled likelihood-based training objectives (Kingma & Welling, 2013). More recently, flow-matching methods (Lipman et al., 2023) have been proposed, which learn the velocity field for a continuous transformation between distributions. Normalizing flows and diffusion-based methods frame generation as transforming a simple reference distribution into the data distribution, either through invertible mappings or stochastic dynamics, and have achieved strong results across many domains (Dinh et al., 2017; Ho et al., 2020). Recent work by (Zhai et al., 2025) further demonstrates that normalizing flows can serve as highly competitive generative models.

Preconditioning. Preconditioning is a classical technique in numerical analysis aimed at improving the conditioning of optimization problems (Ye, 2024) and differential equations (Lazzarino et al., 2025), thereby accelerating convergence and enhancing numerical stability (Saad, 2003; Trefethen & Bau, 1997). By rescaling variables or operators to reduce anisotropy and curvature disparities, preconditioning enables more efficient iterative solvers and more stable time integration (Quirynen & Di Cairano, 2020). Similar issues arise in machine learning, where poorly conditioned objectives can hinder optimization and lead to slow or unstable training dynamics (Cao & Zhang, 2025). Consequently, preconditioning has been widely adopted in large-scale learning systems, both implicitly through adaptive optimization methods and explicitly through problem-dependent transformations, yielding substantial improvements in convergence speed and robustness (Dauphin et al., 2014). In the context of diffusion models, recent work has shown that appropriate reparameterization and noise-dependent preconditioning can substantially improve optimization behavior and sample quality, highlighting the critical role of conditioning in generative model training (Karras et al., 2022).

B. Theoretical Analysis for the Gaussian Transport Model

B.1. Linear Regression Objective and Exact Minimizer

We derive the closed-form solution for the linear regression problem considered in Section 3.3.

We consider a linear predictor for the velocity field at time t ,

$$v_\theta(x_t, t) = A(t) x_t, \quad (26)$$

where $A(t) \in \mathbb{R}^{d \times d}$ is the parameter matrix to be learned. As a proxy for flow or score matching, we take the target velocity

$$v_t^* = x_1 - x_0, \quad (27)$$

and define the mean-squared error loss

$$\mathcal{L}(A(t)) = \mathbb{E}[\|A(t)x_t - (x_1 - x_0)\|^2]. \quad (28)$$

For simplicity, we suppress the explicit dependence on t and write A instead of $A(t)$.

Computing the covariances. Since x_0 and x_1 are independent, zero-mean Gaussians,

$$\mathbb{E}[x_0] = 0, \quad \mathbb{E}[x_1] = 0, \quad \mathbb{E}[x_0 x_1^\top] = 0. \quad (29)$$

By definition,

$$x_t = (1 - t)x_0 + tx_1. \quad (30)$$

The covariance of x_t is therefore

$$\Sigma_t := \mathbb{E}[x_t x_t^\top] \quad (31)$$

$$= \mathbb{E}\left[\left((1 - t)x_0 + tx_1\right)\left((1 - t)x_0 + tx_1\right)^\top\right] \quad (32)$$

$$= (1 - t)^2 \mathbb{E}[x_0 x_0^\top] + t^2 \mathbb{E}[x_1 x_1^\top] + (1 - t) \mathbb{E}[x_0 x_1^\top] + t(1 - t) \mathbb{E}[x_1 x_0^\top]. \quad (33)$$

Using $\mathbb{E}[x_0 x_0^\top] = I$, $\mathbb{E}[x_1 x_1^\top] = H$, and the independence of x_0 and x_1 , we obtain

$$\Sigma_t = (1-t)^2 I + t^2 H. \quad (34)$$

Next, we compute the cross-covariance

$$C := \mathbb{E}[(x_1 - x_0)x_t^\top]. \quad (35)$$

Expanding x_t ,

$$C = (1-t)\mathbb{E}[(x_1 - x_0)x_0^\top] + t\mathbb{E}[(x_1 - x_0)x_1^\top].$$

For the first term,

$$\mathbb{E}[(x_1 - x_0)x_0^\top] = \mathbb{E}[x_1 x_0^\top] - \mathbb{E}[x_0 x_0^\top] = -I, \quad (36)$$

and for the second term,

$$\mathbb{E}[(x_1 - x_0)x_1^\top] = \mathbb{E}[x_1 x_1^\top] - \mathbb{E}[x_0 x_1^\top] = H. \quad (37)$$

Thus,

$$C = tH - (1-t)I. \quad (38)$$

Exact minimizer. Expanding the loss,

$$\mathcal{L}(A) = \mathbb{E}[(Ax_t - (x_1 - x_0))^\top (Ax_t - (x_1 - x_0))]. \quad (39)$$

Using the identity

$$\nabla_A \mathbb{E}[\|Ax - y\|^2] = 2\mathbb{E}[(Ax - y)x^\top], \quad (40)$$

the stationarity condition $\nabla_A \mathcal{L}(A) = 0$ yields

$$A\Sigma_t = C. \quad (41)$$

Since Σ_t is positive definite, the unique minimizer is

$$A^*(t) = C\Sigma_t^{-1} = (tH - (1-t)I)(t^2H + (1-t)^2I)^{-1}. \quad (42)$$

B.2. Spectral Decomposition of Σ_t

We justify the spectral characterization of Σ_t used in Section 3.4. Let $H = U\Lambda U^\top$ be the eigendecomposition of H . Using $I = UIU^\top$, we write

$$\Sigma_t = (1-t)^2 UIU^\top + t^2 U\Lambda U^\top = U((1-t)^2 I + t^2 \Lambda)U^\top. \quad (43)$$

Thus, Σ_t is diagonal in the eigenbasis of H , with eigenvalues

$$\sigma_i(t) = (1-t)^2 + t^2 \lambda_i. \quad (44)$$

B.3. Gradient Descent Error Dynamics

We derive the convergence properties of full batch gradient descent for the linear regression problem.

The gradient of the loss is

$$\nabla_A \mathcal{L}(A) = 2(A\Sigma_t - C), \quad (45)$$

and the gradient descent update with learning rate $\eta > 0$ is

$$A_{k+1} = A_k - 2\eta(A_k \Sigma_t - C). \quad (46)$$

Let A^* be the minimizer and define the error matrix $E_k = A_k - A^*$. Using $A^* \Sigma_t = C$, we obtain

$$E_{k+1} = A_{k+1} - A^* = A_k - 2\eta(A_k \Sigma_t - C) - A^* = E_k - 2\eta E_k \Sigma_t = E_k(I - 2\eta \Sigma_t). \quad (47)$$

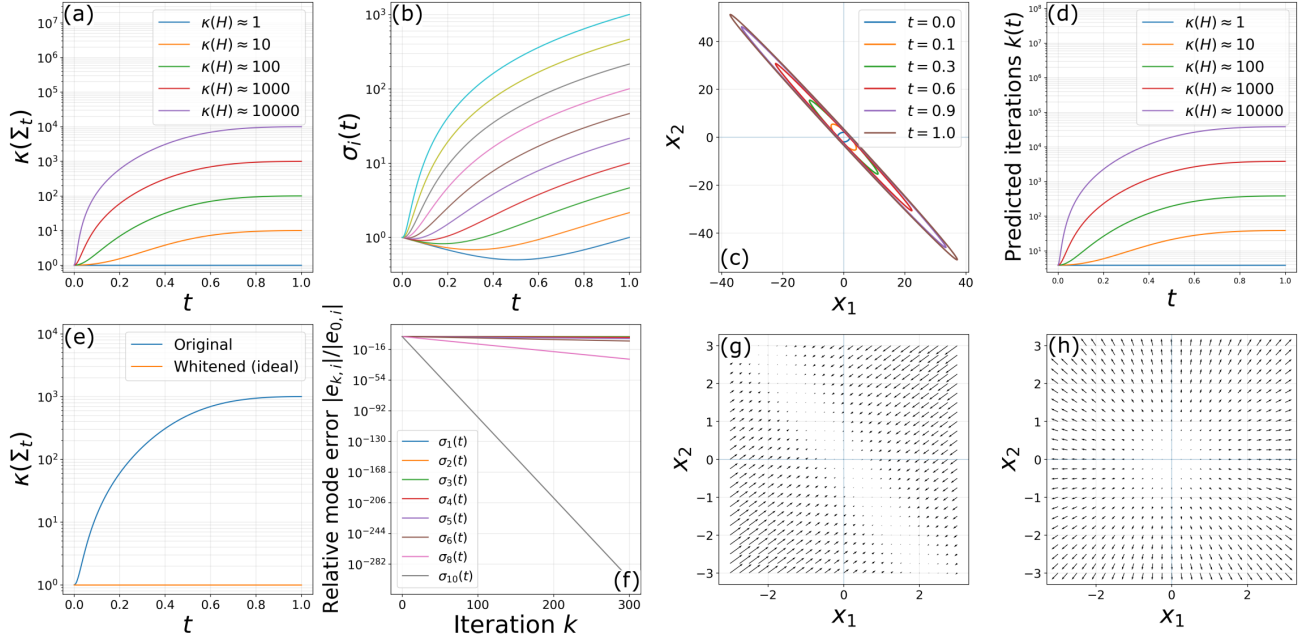


Figure 6. Gaussian model illustrating conditioning and optimization effects in flow and score matching: (a) Growth of the condition number $\kappa(\Sigma_t)$ along the linear interpolation $\Sigma_t = (1-t)^2I + t^2H$ showing how intermediate distributions p_t gradually inherit the ill-conditioning of H ; (b) evolution of the eigenvalues $\sigma_i(t)$ of Σ_t for $\kappa(H) = 1000$, highlighting the increasing spectral disparity that creates slow and fast directions; (c) Covariance ellipses of $p_t = \mathcal{N}(0, \Sigma_t)$ at selected times, visualizing the transition from an isotropic distribution to a highly anisotropic one; (d) Predicted number of gradient-descent iterations $k(t)$ required to reach a fixed error tolerance, demonstrating the sharp slowdown at large t due to ill-conditioning; (e) Effect of ideal preconditioning (whitening), which removes conditioning growth and keeps $\kappa(\Sigma_t) \approx 1$ for all t ; (f) Per-mode gradient-descent error decay at $t = 0.9$, showing that large-variance modes converge rapidly while small-variance modes decay extremely slowly; (g) Optimal score field $s^*(x, t) = -\Sigma_t^{-1}x$, exhibiting strong anisotropy and stiffness along low-variance directions; (h) Optimal flow-matching velocity field $v^*(x, t) = A^*(t)x$, which is smoother than the score but still inherits anisotropy from Σ_t .

Let $\Sigma_t = U \text{diag}(\sigma_1(t), \dots, \sigma_d(t)) U^\top$ be the eigen decomposition of Σ_t . Then

$$I - 2\eta\Sigma_t = U \text{diag}(1 - 2\eta\sigma_1(t), \dots, 1 - 2\eta\sigma_d(t)) U^\top. \quad (48)$$

In the corresponding eigenbasis, each error component evolves independently as

$$e_{i,k+1} = (1 - 2\eta\sigma_i(t)) e_{i,k}. \quad (49)$$

Convergence requires $|1 - 2\eta\sigma_i(t)| < 1$ for all i , which is equivalent to

$$0 < \eta < \frac{1}{\sigma_{\max}(t)}. \quad (50)$$

The slowest decaying mode corresponds to the smallest eigenvalue $\sigma_{\min}(t)$, with contraction factor

$$\rho = 1 - 2\eta\sigma_{\min}(t). \quad (51)$$

To reduce the error in this mode by a factor $\varepsilon \in (0, 1)$, we need approximately

$$k \approx \frac{\log(1/\varepsilon)}{-\log \rho} \approx \frac{1}{2\eta\sigma_{\min}(t)} \log \frac{1}{\varepsilon}, \quad (52)$$

where we used $\log(1-x) \approx -x$ for small x .

B.4. Stochastic Gradient Descent Error Dynamics

This section provides the detailed derivations for the stochastic gradient descent dynamics discussed in Section 3.4.

In practice, we do not have access to the exact expectations defining $\mathcal{L}(A)$ and its gradient; instead, we approximate them using samples and apply stochastic gradient descent (SGD). We analyze the effect of this stochasticity on the error dynamics.

Single sample SGD update. For simplicity, consider SGD updates based on a single sample $(x_0^{(m)}, x_1^{(m)})$ at step m . Define

$$x_t^{(m)} = (1-t)x_0^{(m)} + tx_1^{(m)}, \quad y^{(m)} = x_1^{(m)} - x_0^{(m)}. \quad (53)$$

The per-sample loss is

$$\ell_m(A) = \|Ax_t^{(m)} - y^{(m)}\|^2, \quad (54)$$

and its gradient is

$$\nabla_A \ell_m(A) = 2(Ax_t^{(m)} - y^{(m)})(x_t^{(m)})^\top. \quad (55)$$

The SGD update with learning rate η is

$$A_{m+1} = A_m - \eta \nabla_A \ell_m(A_m) = A_m - 2\eta(A_mx_t^{(m)} - y^{(m)})(x_t^{(m)})^\top. \quad (56)$$

Error recursion with noise. Let A^* denote the exact minimizer and define $E_m = A_m - A^*$. We write the update in terms of E_m :

$$E_{m+1} = A_{m+1} - A^* \quad (57)$$

$$= A_m - 2\eta(A_mx_t^{(m)} - y^{(m)})(x_t^{(m)})^\top - A^*. \quad (58)$$

Add and subtract $2\eta(A^*x_t^{(m)} - y^{(m)})(x_t^{(m)})^\top$ to obtain

$$E_{m+1} = A_m - A^* \quad (59)$$

$$- 2\eta \left[(A_mx_t^{(m)} - y^{(m)}) - (A^*x_t^{(m)} - y^{(m)}) \right] (x_t^{(m)})^\top \quad (60)$$

$$= E_m - 2\eta(A_mx_t^{(m)} - y^{(m)})(x_t^{(m)})^\top \quad (61)$$

$$+ 2\eta(A^*x_t^{(m)} - y^{(m)})(x_t^{(m)})^\top \quad (62)$$

$$= E_m - 2\eta E_mx_t^{(m)}(x_t^{(m)})^\top - 2\eta(A^*x_t^{(m)} - y^{(m)})(x_t^{(m)})^\top. \quad (63)$$

Taking expectations conditional on E_m and using

$$\mathbb{E}[x_t^{(m)}(x_t^{(m)})^\top] = \Sigma_t, \quad \mathbb{E}[A^*x_t^{(m)} - y^{(m)}] = 0, \quad (64)$$

we recover the deterministic contraction

$$\mathbb{E}[E_{m+1} | E_m] = E_m(I - 2\eta\Sigma_t), \quad (65)$$

as in the full batch case. The last term

$$\xi_m := -2\eta(A^*x_t^{(m)} - y^{(m)})(x_t^{(m)})^\top \quad (66)$$

is a zero-mean noise term (since A^* satisfies the optimality condition) that represents gradient variability.

We can therefore write the SGD error recursion as

$$E_{m+1} = E_m(I - 2\eta\Sigma_t) + \Xi_m, \quad (67)$$

where Ξ_m is a zero-mean random matrix capturing gradient noise. Projecting onto any eigen direction i of Σ_t , the corresponding scalar error component $e_{i,m}$ satisfies

$$e_{i,m+1} = (1 - 2\eta\sigma_i(t))e_{i,m} + \zeta_{i,m}, \quad (68)$$

where $\zeta_{i,m}$ is a zero-mean noise term whose variance depends on the gradient variance in direction i .

Steady state variance. For a scalar recursion

$$z_{m+1} = az_m + \xi_m, \quad (69)$$

with $|a| < 1$, zero mean noise ξ_m of variance $\text{Var}(\xi_m) = \sigma_\xi^2$, and ξ_m independent across m , the stationary variance is

$$\text{Var}(z_\infty) = \frac{\sigma_\xi^2}{1 - a^2}. \quad (70)$$

In our case, $a = 1 - 2\eta\sigma_i(t)$, so

$$1 - a^2 = 1 - (1 - 2\eta\sigma_i(t))^2 = 4\eta\sigma_i(t) - 4\eta^2\sigma_i(t)^2. \quad (71)$$

For small η , the term $4\eta^2\sigma_i(t)^2$ is negligible compared to $4\eta\sigma_i(t)$, yielding the approximation

$$1 - a^2 \approx 4\eta\sigma_i(t). \quad (72)$$

If we denote by $\sigma_{\zeta,i}^2$ the variance of the noise $\zeta_{i,m}$, the stationary variance of $e_{i,m}$ is

$$\text{Var}(e_{i,\infty}) \approx \frac{\sigma_{\zeta,i}^2}{4\eta\sigma_i(t)}. \quad (73)$$

Since $\sigma_{\zeta,i}^2$ scales proportionally to η^2 , we may write $\sigma_{\zeta,i}^2 \approx c_i\eta^2$ for constants c_i depending on the data distribution and A^* . Substituting,

$$\text{Var}(e_{i,\infty}) \approx \frac{c_i\eta^2}{4\eta\sigma_i(t)} = \frac{c_i\eta}{4\sigma_i(t)}. \quad (74)$$

Thus, up to constants, the steady state variance in direction i scales as

$$\text{Var}(e_{i,\infty}) \propto \frac{\eta}{\sigma_i(t)}. \quad (75)$$

Implications. Directions with small $\sigma_i(t)$ therefore suffer a double disadvantage. First, the contraction factor $1 - 2\eta\sigma_i(t)$ is close to one, so the bias in that direction decays very slowly. Second, the steady state variance $\text{Var}(e_{i,\infty})$ scales inversely with $\sigma_i(t)$, so low variance directions accumulate larger stochastic fluctuations for a given learning rate. Together, these effects make low eigenvalue modes the bottleneck in both convergence speed and final accuracy, mirroring the behavior of SGD on ill-conditioned quadratic objectives.

C. Theoretical Analysis of the Gaussian Mixture Model

This section provides the full derivations underlying the Gaussian mixture model extension discussed in Section 3.5 of the main text.

We now extend the analysis to the setting where the target distribution is a mixture of Gaussians. This case introduces multimodality and provides a stylized model for real datasets that contain clusters or discrete semantic modes. Importantly, as in the single-Gaussian case, the score and probability–flow velocity remain analytic, which enables exact characterization of the optimization dynamics.

C.1. Analytic Velocity and Score in the GMM Case

Let the target distribution be a mixture of K zero-mean Gaussians

$$x_1 \sim \sum_{k=1}^K \pi_k \mathcal{N}(0, H_k), \quad \pi_k > 0, \quad \sum_{k=1}^K \pi_k = 1, \quad (76)$$

and let the base distribution remain

$$x_0 \sim \mathcal{N}(0, I), \quad (77)$$

with interpolation

$$x_t = (1 - t)x_0 + tx_1. \quad (78)$$

We denote the component posterior weights at time t

$$w_k(x_t) := \mathbb{P}(x_1 \text{ originated from component } k \mid x_t), \quad (79)$$

which satisfy $\sum_k w_k(x_t) = 1$ and depend on both π_k and H_k .

Score. Since x_t is a mixture of Gaussians,

$$p_t(x_t) = \sum_{k=1}^K \pi_k \mathcal{N}(0, \Sigma_{t,k}), \quad \Sigma_{t,k} = (1 - t)^2 I + t^2 H_k, \quad (80)$$

and the score admits the usual mixture-of-Gaussians form

$$\nabla_x \log p_t(x_t) = - \sum_{k=1}^K w_k(x_t) \Sigma_{t,k}^{-1} x_t. \quad (81)$$

Velocity. The probability-flow ODE again satisfies $\frac{dx_t}{dt} = x_1 - x_0$, so conditioning on x_t and using the mixture law of total expectation gives

$$v_t^*(x_t) = \mathbb{E}[x_1 - x_0 \mid x_t] = \sum_{k=1}^K w_k(x_t) A_k^*(t) x_t, \quad (82)$$

with

$$A_k^*(t) = (tH_k - (1 - t)I)((1 - t)^2 I + t^2 H_k)^{-1}. \quad (83)$$

Thus, the analytic velocity is a *mixture of linear maps* applied to x_t , weighted by $w_k(x_t)$.

Key observation. Unlike the single-Gaussian case where the velocity is purely linear in x_t , the velocity here is a *linear mixture with data-dependent component weights*. The exact flow is still structured and low-dimensional, but no single linear matrix $A(t)$ can represent it in general.

C.2. Learning a Mixture of Linear Predictors

To focus on optimization rather than model misspecification, we assume that the model has the correct number of mixture components and that the mixture means are known. We parameterize

$$v_\theta(x_t, t) = \sum_{k=1}^K \hat{w}_k(x_t) A_k(t) x_t, \quad (84)$$

where $A_k(t) \in \mathbb{R}^{d \times d}$ and $\hat{w}_k(x_t)$ are estimated mixture responsibilities. For simplicity, and to isolate conditioning effects, we assume $\hat{w}_k(x_t) = w_k(x_t)$ (perfect gating). The regression objective becomes

$$\mathcal{L}(\{A_k(t)\}) = \mathbb{E} \left[\left\| \sum_{k=1}^K w_k(x_t) A_k(t) x_t - (x_1 - x_0) \right\|^2 \right]. \quad (85)$$

As before, define the optimal matrices via

$$A_k^*(t) = (tH_k - (1 - t)I)((1 - t)^2 I + t^2 H_k)^{-1}, \quad (86)$$

so the model class is again expressive enough to represent the exact analytic velocity. Any observed optimization difficulty arises solely from the induced regression structure, not from lack of capacity.

C.3. Conditioning of the Regression Problem

Since gradients with respect to A_k are taken only on samples effectively routed to component k , the subproblem for A_k is governed by the covariance of x_t conditional on component k :

$$\Sigma_{t,k} = \mathbb{E}[x_t x_t^\top \mid x_1 \text{ in component } k] = (1-t)^2 I + t^2 H_k. \quad (87)$$

Diagonalizing $H_k = U_k \Lambda_k U_k^\top$, we obtain eigenvalues

$$\sigma_{k,i}(t) = (1-t)^2 + t^2 \lambda_{k,i}, \quad i = 1, \dots, d. \quad (88)$$

The condition number within component k is therefore

$$\kappa(\Sigma_{t,k}) = \frac{(1-t)^2 + t^2 \lambda_{k,\max}}{(1-t)^2 + t^2 \lambda_{k,\min}}. \quad (89)$$

Just as in the single-Gaussian case, $\kappa(\Sigma_{t,k})$ grows rapidly with both t and the condition number $\kappa(H_k) = \lambda_{k,\max}/\lambda_{k,\min}$.

Coupling across components. The overall optimization landscape combines K subproblems with potentially very different condition numbers. Modes belonging to poorly conditioned components (small $\lambda_{k,\min}$) converge much more slowly than those belonging to well-conditioned components. Thus, the global convergence rate of the whole model is governed by

$$\min_{k,i} \sigma_{k,i}(t), \quad (90)$$

i.e. by the *hardest* direction across *all* mixture components.

C.4. Gradient Descent Error Dynamics

Let $A_k^*(t)$ denote the optimal matrices and define error matrices $E_{k,\ell} = A_{k,\ell} - A_k^*(t)$ at iteration ℓ . The gradient of \mathcal{L} with respect to A_k contracts each $E_{k,\ell}$ according to

$$E_{k,\ell+1} = E_{k,\ell} (I - 2\eta \Sigma_{t,k}), \quad (91)$$

so in eigen-direction i of component k ,

$$e_{k,i,\ell+1} = (1 - 2\eta \sigma_{k,i}(t)) e_{k,i,\ell}. \quad (92)$$

Convergence requires

$$0 < \eta < \frac{1}{\max_{k,i} \sigma_{k,i}(t)}, \quad (93)$$

and the number of gradient steps needed to reduce the slowest mode by a factor ε is

$$\frac{1}{2\eta \min_{k,i} \sigma_{k,i}(t)} \log \frac{1}{\varepsilon}. \quad (94)$$

Thus, even if most mixture components are well-conditioned, a single poorly conditioned component controls the global training speed.

C.5. Stochastic Gradient Descent Error Dynamics

With minibatch SGD and perfect gating, the SGD update for A_k depends only on samples assigned to component k . The scalar error in eigen-direction i of component k follows the stochastic recursion

$$e_{k,i,m+1} = (1 - 2\eta \sigma_{k,i}(t)) e_{k,i,m} + \zeta_{k,i,m}, \quad (95)$$

with zero-mean noise $\zeta_{k,i,m}$. As in the single-Gaussian case, the stationary variance satisfies

$$\text{Var}(e_{k,i,\infty}) \propto \frac{\eta}{\sigma_{k,i}(t)}, \quad (96)$$

so directions with small $\sigma_{k,i}(t)$ exhibit both:

- extremely slow bias decay (contraction factor near 1), and
- large steady-state variance accumulated from SGD noise.

Consequently, the global convergence rate and final error are governed by the *worst* (smallest) eigenvalue among *all* mixture components.

Summary. Even when the model has the correct number of components and perfect component allocation, optimization is bottlenecked by the lowest-variance directions of the hardest mixture component. The Gaussian mixture case, therefore, makes the failure mode more pronounced: training cannot converge faster than the most ill-conditioned component permits.

D. Preconditioning

D.1. Proof of Theorem 4.1 – Preconditioning Improves Convergence

We consider the linear regression objective,

$$\mathcal{L}(A) = \mathbb{E}[\|Ax - y\|^2], \quad (97)$$

where $\Sigma = \mathbb{E}[xx^\top]$ is the input covariance matrix, assumed positive definite with condition number $\kappa(\Sigma) = \lambda_{\max}(\Sigma)/\lambda_{\min}(\Sigma)$.

Non-Preconditioned Case. Let $C = \mathbb{E}[yx^\top]$. Then the objective expands as,

$$\mathcal{L}(A) = \text{Tr}(A\Sigma A^\top) - 2\text{Tr}(AC^\top) + \mathbb{E}[\|y\|^2], \quad (98)$$

and the gradient is,

$$\nabla \mathcal{L}(A) = 2A\Sigma - 2C. \quad (99)$$

The optimal solution satisfies $A^* = C\Sigma^{-1}$. Define the error matrix $E_k = A_k - A^*$, and write the gradient descent update as,

$$E_{k+1} = E_k - 2\eta E_k \Sigma. \quad (100)$$

Let $\Sigma = U\Lambda U^\top$ be the eigendecomposition of Σ with $\Lambda = \text{diag}(\lambda_1, \dots, \lambda_d)$. Let $\tilde{E}_k = E_k U$. Then,

$$\tilde{E}_{k+1} = \tilde{E}_k (I - 2\eta \Lambda), \quad (101)$$

so each column evolves as,

$$\tilde{E}_k^{(i)} = (1 - 2\eta \lambda_i)^k \tilde{E}_0^{(i)}. \quad (102)$$

Thus,

$$\|E_k\|_F \leq (1 - 2\eta \lambda_{\min}(\Sigma))^k \|E_0\|_F. \quad (103)$$

To achieve $\|E_k\|_F \leq \varepsilon$, we need,

$$k \geq \frac{1}{2\eta \lambda_{\min}(\Sigma)} \log \left(\frac{\|E_0\|_F}{\varepsilon} \right). \quad (104)$$

Since stable convergence requires $\eta \leq 1/\lambda_{\max}(\Sigma)$ (meaning $\eta \sim \mathcal{O}(1/\lambda_{\max})$), the number of steps scales as,

$$k = \mathcal{O}(\kappa \log(1/\varepsilon)). \quad (105)$$

Preconditioned Case. Let $\mathcal{P} = \Sigma^{-1/2}$, and define $\tilde{x} = \mathcal{P}x$. Then $\mathbb{E}[\tilde{x}\tilde{x}^\top] = I$, and we minimize,

$$\tilde{\mathcal{L}}(A) = \mathbb{E}[\|A\tilde{x} - y\|^2], \quad (106)$$

whose gradient is $\nabla \tilde{\mathcal{L}}(A) = 2A - 2\tilde{C}$, where $\tilde{C} = \mathbb{E}[y\tilde{x}^\top]$. The solution is $A^* = \tilde{C}$, and gradient descent becomes,

$$A_{k+1} = A_k - 2\eta(A_k - A^*) \Rightarrow E_{k+1} = (1 - 2\eta)E_k. \quad (107)$$

Hence,

$$\|E_k\|_F = (1 - 2\eta)^k \|E_0\|_F. \quad (108)$$

This convergence is uniform in all directions and independent of κ . Choosing $\eta = 1/2$ yields,

$k = \mathcal{O}(\log(1/\varepsilon)).$

(109)

This completes the proof.

D.2. Preconditioning for Gaussian Mixtures

This subsection provides the detailed construction underlying Gaussian mixture preconditioning, referenced in Section 4 of the main text.

For a mixture

$$x_1 \sim \sum_{k=1}^K \pi_k \mathcal{N}(0, H_k), \quad (110)$$

the ill-conditioning arises not only from the spread of eigenvalues within each H_k , but also from imbalance across components. A component with small variance in one direction can dominate convergence time, even if all other components are well-conditioned.

To address this, we define a blockwise transform that whitens each component individually. For each k , let $H_k = U_k \Lambda_k U_k^\top$ and define

$$T_k = \Lambda_k^{-1/2} U_k^\top. \quad (111)$$

We map the original distribution to

$$\tilde{x}_1 \sim \sum_{k=1}^K \pi_k \mathcal{N}(0, I), \quad (112)$$

i.e. a mixture with identical isotropic components. Training proceeds on the preconditioned interpolation

$$\tilde{x}_t = (1 - t)x_0 + t\tilde{x}_1, \quad (113)$$

with a velocity model

$$\tilde{v}_\theta(\tilde{x}_t, t) = \sum_{k=1}^K \hat{w}_k(\tilde{x}_t) \tilde{A}_k(t) \tilde{x}_t, \quad (114)$$

and the analytic solution satisfies

$$\tilde{A}_k^*(t) = \frac{t - (1 - t)}{(1 - t)^2 + t^2} I \quad \text{for all } k. \quad (115)$$

Thus, after preconditioning, all mixture components become identical and perfectly conditioned. The global optimization bottleneck is eliminated: no component can dominate convergence by having unusually small variance in some direction.

After learning \tilde{v}_θ , the corresponding velocity in the original space is obtained via the inverse transforms:

$$v_\theta(x_t, t) = \sum_{k=1}^K \hat{w}_k(x_t) T_k^{-1} \tilde{A}_k(t) T_k x_t. \quad (116)$$

D.3. Effect on Conditioning and Convergence

This subsection provides the detailed conditioning and convergence analysis for Gaussian mixture preconditioning referenced in Section 4 of the main text.

Let $\sigma_{k,i}(t)$ denote the eigenvalues of the matrices $\Sigma_{t,k}$ in the original space. Let $\tilde{\sigma}_{k,i}(t)$ denote the eigenvalues after preconditioning. By construction,

$$\tilde{\sigma}_{k,i}(t) = (1-t)^2 + t^2 \quad \text{independent of } k, i, \quad (117)$$

so

$$\kappa(\tilde{\Sigma}_{t,k}) = 1 \quad \text{for all } k, t. \quad (118)$$

Therefore

- gradient descent converges at a uniform rate across all directions, and
- the steady-state variance under SGD is the same in every direction.

No single mode or mixture component can slow down training. The convergence rate is now determined solely by the learning rate and batch size, rather than by geometric properties of the data distribution.

E. Qualitative Comparison of Flow-Based Preconditioning

E.1. MNIST

We provide qualitative comparison for the flow matching in the latent space of an MNIST-trained VAE (latent dimension 64, see Section F.1 for details) when the latent space was not preconditioned (left) (FID=13.8269), preconditioned using a normalizing flow (middle) (FID=2.6223), and preconditioned using a flow matching model (right) (FID=6.9544) in Figure 7. The visual quality of the samples is consistent with the FID scores, with sharper and more coherent digits observed in the preconditioned cases. We also analyzed the condition number dynamics as a function of time t during the training of these flow models, which are presented in Figure 12.

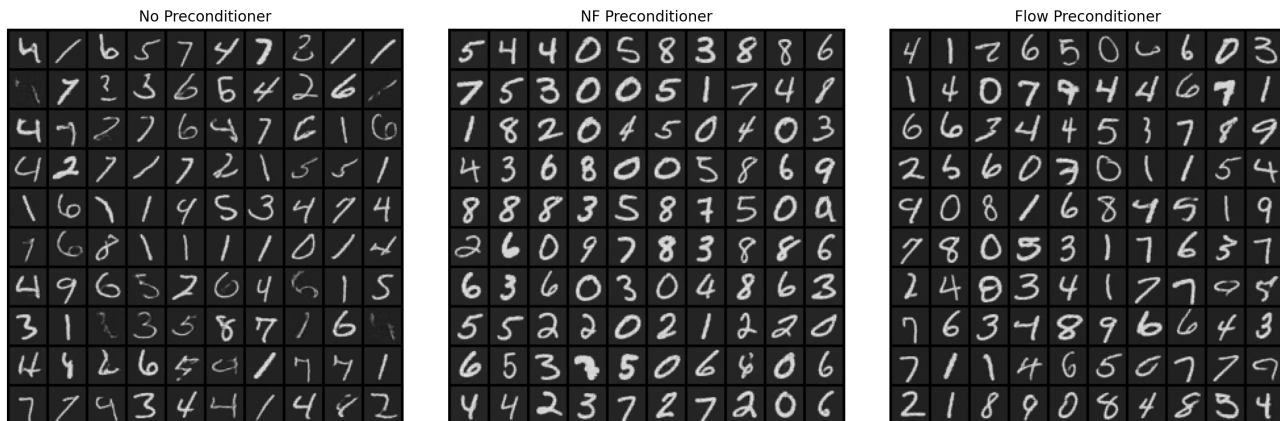


Figure 7. MNIST qualitative comparison. Comparison of MNIST samples generated by flow matching in latent space under different preconditioning strategies. **Left:** No preconditioning results in blurry and inconsistent digit shapes (FID = 13.83). **Middle:** Preconditioning with a normalizing flow improves digit clarity and diversity (FID = 2.62). **Right:** Preconditioning with a learned flow matching model also improves sample quality over the baseline (FID = 6.95). Visual quality trends align with quantitative FID scores.

E.2. High-Resolution Images

We provide qualitative comparisons illustrating the effect of flow-based preconditioning on sample quality for Oxford Flowers-102 (Nilsback & Zisserman, 2008), LSUN Churches (Yu et al., 2015), and AFHQ Cats (Choi et al., 2020). As shown in Figures 8 to 10, these examples complement the quantitative improvements reported in Table 3 and illustrate how the additional flow improves sample consistency in cases where standard flow matching remains visually imperfect.

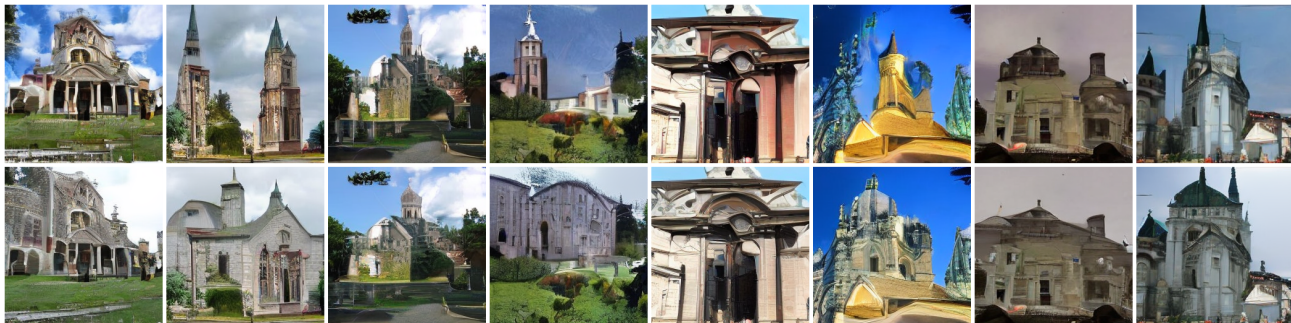


Figure 8. **LSUN Churches qualitative comparison.** Samples generated by standard flow matching (*top*) and by flow-based preconditioning using an additional flow (*bottom*). Preconditioning produces a sharper global structure and more stable spatial layouts.



Figure 9. **Oxford Flowers-102 qualitative comparison.** Samples generated by standard flow matching (*top*) and by flow-based preconditioning using an additional flow (*bottom*). Preconditioning yields more coherent structure and improved visual consistency.



Figure 10. **AFHQ Cats qualitative comparison.** Samples generated by standard flow matching (*top*) and by flow-based preconditioning using an additional flow (*bottom*).

F. Experimental Details

F.1. MNIST

We evaluate our preconditioning strategy on MNIST using a two-stage approach in the latent space of a VAE. This VAE consisted of a deep ResNet-based architecture with group normalization, SiLU activations, and was trained using a combination of MSE and perceptual loss. The encoder and decoder consist of multiple downsampling and upsampling ResBlocks, with a latent dimensionality of 64. Training uses cosine learning rate decay, KL regularization with low $\beta = 0.05$.

Once trained, the VAE maps MNIST images to latent vectors $x_1 \in \mathbb{R}^{64}$, and our goal is to learn a generative model that transports Gaussian noise $z \sim \mathcal{N}(0, 1)$ to this latent distribution via flow matching. The main flow model is a conditional vector field implemented as a fully connected MLP. It takes as input, (i) a latent vector x_t interpolated between x_1 and x_0 via $x_t = \sin(\frac{\pi}{2}t)x_1 + \cos(\frac{\pi}{2}t)x_0$, (ii) time t , and (iii) one-hot encoded class label y . We compare three variants:

1. No preconditioning: Standard flow matching from Gaussian to data in the latent space of the trained VAE.
2. Normalizing Flow Preconditioner: A reversible MLP trained with maximum-likelihood to Gaussianize the VAE latent codes.
3. Reduced-capacity Flow Preconditioner: A flow model trained via flow matching using limited training epochs to push the latent codes closer to Gaussian.

For quantitative evaluation, we decode generated latent vectors using the VAE decoder and compute FID scores between generated and real MNIST images using our own trained class-conditional MNIST classifier.

The architectural details for the preconditioner networks are explained in detail below:

- **Normalizing Flow Preconditioner.** The normalizing flow (NF) preconditioner is implemented as a reversible MLP-based model designed to map the latent distribution of the VAE to a standard Gaussian. Specifically, we use a sequence of affine coupling layers based on the RealNVP architecture (Dinh et al., 2017). Each coupling layer splits the input latent vector into two parts: one half is left unchanged, while the other is transformed via a learnable scale-and-shift operation conditioned on the fixed part. The scale and shift functions are parameterized by shallow MLPs with two hidden layers of 256 units and ReLU activations. To improve expressiveness, we alternate the partitioning pattern across layers and insert random permutations between them. The full NF model consists of 6 such coupling layers. This architecture is trained with maximum-likelihood using the standard change-of-variables formula, optimizing the log-likelihood of the VAE latent codes under the transformed Gaussian distribution (Kobyzev et al., 2020).
- **Flow Matching Preconditioner.** The flow-based preconditioner is implemented as a class-conditional vector field modeled by an MLP with input dimensions corresponding to the latent vector x_t , t , and class label y . The MLP uses two hidden layers with 128 units and ReLU activations. This architecture is identical to the main flow model used in stage two. Unlike the normalizing flow, this preconditioner is trained using the flow matching objective to push VAE latents toward Gaussian noise. However, instead of using a smaller architecture, we simulate reduced capacity by limiting the number of training epochs to just 300 (as opposed to 1000 epochs for training the second stage flow model), resulting in a less accurate but computationally inexpensive preconditioner. The training uses sinusoidal interpolation, and samples are matched against Gaussian noise via the standard flow matching loss.

The remaining experimental details for training the main flow model for MNIST are summarized in Table 4.

Table 4. Experimental settings and hyperparameters for the main flow model in MNIST.

MNIST	
Model	Conditional MLP
Image size (1-channel)	28×28
Max Epochs	1000
Learning rate	2×10^{-4}
Optimizer	AdamW
Batch size	4096
Hidden layers	2
Hidden dimensions	128
Interpolation	$s(t) = \sin(\frac{\pi}{2}t), c(t) = \cos(\frac{\pi}{2}t)$

F.2. High-Resolution Image Synthesis

We evaluate our method on the Oxford Flowers-102 (Nilsback & Zisserman, 2008), LSUN Churches (Yu et al., 2015), and AFHQ Cats (Choi et al., 2020) datasets. All experiments are conducted in the latent space of a pretrained VAE, using the Stable Diffusion VAE encoder–decoder (Rombach et al., 2022). This model spatially compresses by a factor of 8, giving a 4×32 latent representation for 256^2 images (Flowers, Churches) and a $4 \times 64 \times 64$ representation for 512^2 images (AFHQ Cats). We compare standard flow matching in latent space with a preconditioned variant that employs an additional flow model. The architecture and training details of the baseline flow model are summarized in Table 5.

The architectural details for the preconditioner network are explained in detail below:

- **Flow Matching Preconditioner.** Preconditioning is implemented using an additional flow model operating in the same latent space. The preconditioner uses the same UNet architecture as the main flow model, but is trained with reduced accuracy by limiting the number of training epochs to at most one-third of the main flow-matching training budget. This yields a computationally inexpensive transformation that partially Gaussianizes the latent data distribution while preserving semantic structure. A matching-point operator is applied between the preconditioning flow and the main flow to ensure consistent alignment of intermediate distributions and stable composition of the learned transports.

The preconditioning flow is trained first and then frozen. The main flow model is subsequently trained on the preconditioned latent distribution using the same optimization settings as the baseline. Sample quality is evaluated by decoding generated latent samples back to image space and computing FID against real images.

Table 5. Experimental settings and hyperparameters for LSUN Churches, Oxford Flowers-102, and AFHQ Cats datasets.

	LSUN Churches	Oxford Flowers-102	AFHQ Cats
Model	UNet	UNet	Unet
Image size (3-channel)	256×256	256×256	512×512
Max Epochs	150	300	800
Learning rate	5×10^{-5}	5×10^{-5}	1×10^{-4}
Optimizer	AdamW	AdamW	AdamW
Batch size	32	32	32 (16 × 2)
Hidden Layers	256	256	192
Attention heads	4	4	12-24
Blocks	3	3	2

G. Additional Experiments and Results

G.1. Transport from Checkerboard to Swiss Roll: 2D → 1D Manifold Transport

To provide a controlled visualization of the optimization effects discussed above, we consider a two-dimensional transport task from a checkerboard source distribution p_0 to a Swiss roll target distribution p_1 , which lies on a lower-dimensional manifold. This setting isolates geometric and optimization effects independently of high-dimensional model capacity and allows direct inspection of learned transport trajectories.

Figure 11 compares flow matching without and with preconditioning. Without preconditioning, the learned transport exhibits distorted and highly anisotropic trajectories, with many samples failing to align with the target manifold. Although the training loss decreases, optimization stagnates early, resulting in poor target coverage and a relatively high final distributional discrepancy. In contrast, preconditioning reshapes the source geometry before transport, yielding smoother and more coherent flow lines and substantially improved alignment of the transported samples \hat{p}_1 with the Swiss roll target.

The right panel quantifies this behavior using the MMD metric. While both models initially reduce the discrepancy, the unpreconditioned model plateaus early, whereas the preconditioned model continues to make progress and converges to a significantly lower final MMD. This example illustrates that preconditioning does not necessarily accelerate early convergence, but instead mitigates optimization stagnation by enabling continued progress along directions that are otherwise suppressed by ill-conditioning, consistent with the conditioning-based analysis developed in earlier sections.

G.2. Condition Number Dynamics for MNIST Training

To understand how preconditioning impacts the geometry of the transport process, we measure the condition number $\kappa(\Sigma_t)$ of the covariance matrix of samples x_t from the intermediate distributions p_t at various time steps $t \in (0, 1)$ during the flow matching training for the MNIST dataset. A higher condition number indicates stronger anisotropy, which typically hinders optimization during flow matching.

Figure 12 shows that without preconditioning, the condition number increases rapidly with time t , indicating poor conditioning. Both the normalizing flow and flow matching preconditioners significantly reduce the condition numbers across

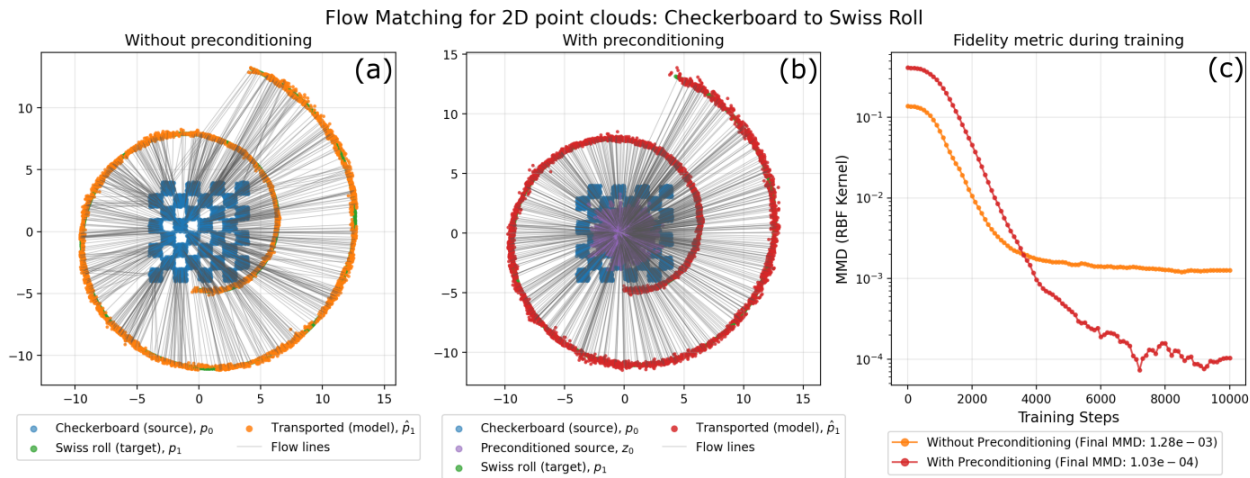


Figure 11. Effect of preconditioning in flow matching for a Checkerboard \rightarrow Swiss Roll transport (2D \rightarrow 1D manifold transport). Flow matching transports samples from a checkerboard source p_0 to a Swiss-roll target p_1 . (a) Without preconditioning, the learned transport shows distorted trajectories and poor target coverage. (b) With preconditioning, the normalized source yields smoother flows and more accurate alignment of the transported samples \hat{p}_1 with p_1 . (c) Preconditioning prevents early optimization stagnation and enables continued reduction in distributional discrepancy, achieving a substantially lower final MMD than the unpreconditioned model.

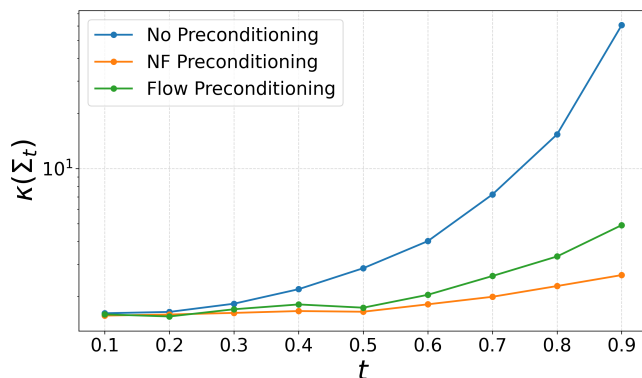


Figure 12. Condition number $\kappa(\Sigma_t)$ of the intermediate distributions p_t over time t during flow matching on MNIST latent space. Without preconditioning (blue), the covariance matrices Σ_t become increasingly ill-conditioned as $t \rightarrow 1$, impeding optimization. Both normalizing flow (NF) (orange) and flow matching (green) preconditioning significantly reduce condition numbers, especially for large t , improving numerical stability and convergence.

all t , with the normalizing flow achieving the most isotropic intermediate representations, which is also reflected in the quantitative results obtained for MNIST in Table 2. These results highlight the effectiveness of preconditioning in improving optimization geometry during training.